PERFORMANCE ASSESSMENT OF INTRA-DAY SOLAR IRRADIATION FORECAST IN URUGUAY USING SATELLITE CLOUD MOTION VECTORS

Gianina Giacosa[1] and Rodrigo Alonso-Suárez[2]

[1] Instituto Uruguayo de Meteorología, Montevideo (Uruguay)

[2] Laboratorio de Energía Solar, Universidad de la República, Montevideo (Uruguay)

Abstract

Reliable solar irradiation forecast is increasingly important for solar PV power dispatch. Satellite forecasting methods are suitable for the intra-day time horizons. In this work we evaluate the performance of the satellite cloud motion vector (CMV) forecasting technique proposed by Lorenz et al. (2004) for the Uruguayan territory. The local implementation of this technique is also presented in this article. The performance assessment is done for the prediction of the hourly solar global irradiation at ground level from 1 to 5 hours ahead and for site and regional forecast. As expected, the root mean square deviation (RMSD) of the regional CMV technique is significantly lower than over specific sites, with values ranging from 9% to 18% for the former and from 19% to 37% for the latter. Positive forecasting skills (FS) are obtained for all the inspected time horizons in both spatial scales (site and regional). The FS metric peaks at +16% for site forecast (at 2 hours ahead) and at +30% for regional forecast (at 4 hours ahead).

Keywords: solar irradiation, forecast, satellite images, GOES-East.

1. Introduction

Since the year 2017 there are 230MW of large-scale grid-connected solar photovoltaic (PV) power installed in Uruguay, representing 5% of the total installed capacity in the country (ADME, 2018). PV power contribution is expected to grow significantly during this decade due to new installations (Gurín et al., 2016). As a consequence, reliable locally-adapted PV power forecast at the useful time horizons for load dispatch is of increasing importance for grid management. While intra-hour forecast is relevant for automatic load following, intra-day forecast is important for managing multiple load zones and energy exports (Pedro and Coimbra, 2012). These are the time horizons where solar satellite forecasting techniques can be exploited, being an important source of information due to the images' temporal and spatial resolution (Lorenz et al., 2004).

Solar satellite forecast is done by estimating and extrapolating the movement of clouds from geostationary satellite imagery, usually, by using the last two available images. This is possible because the rate of the images is typically of 15 or 30 minutes depending on the satellite capabilities. The cloud's movement is represented by a two dimensional vector field known as Cloud Motion Vectors (CMV) or Cloud Motion Field (CMF), which is estimated from the sequence of images. The estimated CMV is used to extrapolate the near future position of clouds (i.e. from minutes to some hours ahead). Then, by using a solar satellite assessment model, it is possible to predict the ground level solar irradiation. This family of techniques reduces the clouds' three dimensional physical problem into a two dimensional displacement problem, thus the forecast is prone to deviations that arise from this simplification. For instance, these techniques are incapable of forecasting the complicated convection processes in clouds. However, the CMV techniques have proved to be a suitable solar forecasting technique (Kühnert et al., 2013; Perez and Hoff, 2013), providing better forecasting accuracy than the Numerical Weather Predictions for forecast horizons up to 4 hours ahead. Also, solar satellite forecast has proved to beat the persistence procedure performance, typically, from 2 hours ahead and above.

In this work we implement locally and assess the performance of a satellite CMV forecasting technique to predict global solar irradiation at ground level (GHI) up to 5 hours ahead. The CMV estimation is based on the similarity of regions in two consecutive images as proposed by Lorenz et al., 2004. The performance of the method is compared with the standard persistence procedure, both for site and regional forecast. This is the first performance evaluation of a satellite-based CMV solar forecasting method in the region and, for the best of our knowledge, in Latin America. This article is organized in the following way. Section 2 describes the data, namely, the solar irradiation ground measurements and the GOES-East satellite images. Section 3 explains the CMV forecasting methodology implemented in this work and Section 4 presents its results. Finally, Section 5 summarizes our conclusions.

2. Data

2.1. Solar irradiation measurements

The reference GHI ground measurements were registered in seven sites distributed across the Uruguayan territory. The location of the ground stations are presented in Tab. 1 and illustrated in Fig. 1. The region under study is classified in the Köppen-Geiger climate classification (Peel et al., 2007) as Cfb (temperate, without dry season, warm summers) in the southeast area influenced by the Atlantic Ocean and Cfa (temperate, without dry season, hot summers) in the inner part of the country. This area is representative of the broader Pampa Humeda region of south-east of South America.

One of the sites is located at an experimental facility of the Solar Energy Laboratory where high quality ground measurements are maintained (LE site). This station is equipped with a Kipp & Zonen Solys2 ground station and the GHI measurement is done using a Secondary Standard pyranometer (according to the ISO 9060:2018 standard). The other six stations are part of the field measurements network (RMCIS) administrated by this Laboratory. The GHI measurements in these sites are taken with First Class or Secondary Standard pyranometers. All the pyranometers are calibrated every two years as recommended by the WMO (World Meteorological Organization), using a Kipp & Zonen CMP22 Secondary Standard. This instrument has traceability to the World Radiometric Reference in Davos, Switzerland. Measurements are registered at a 1-minute rate as the average of 15 seconds instantaneous samples. The hourly irradiation records required for this work were obtained by integrating the 1 minute measurements. The hourly integrals follow the South America GOES-East satellite time stamp, which will be explained in the next Subsection.

Tab. 1: Information from ground stations.

code	latitude (deg)	longitud (deg)	altitude (m)
LE	-31.28	-57.92	42
PP	-33.26	-54.49	58
RC	-34.49	-54.32	24
AR	-30.40	-56.51	136
LB	-34.67	-56.34	32
TA	-33.71	-55.83	140
ZU	-34.34	-57.69	81

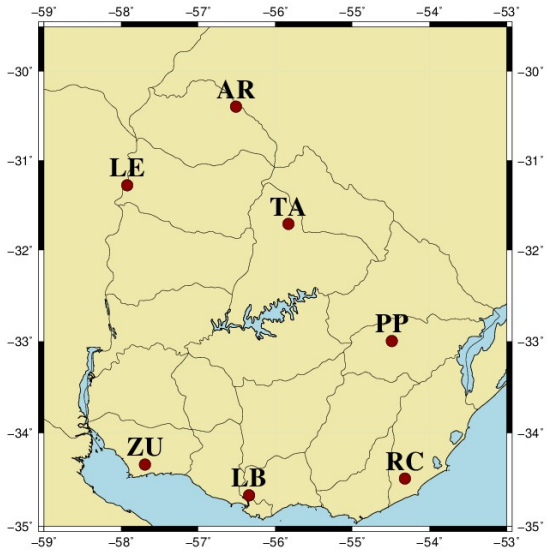

Fig.1: Ground stations distribution across the Uruguayan territory.

2.2. Satellite images

Visible channel GOES-East satellite images from January 2016 to December 2017 are used in this work, comprising two complete years of the former GOES13 satellite. During this period, satellite images for South America had an irregular acquisition regime. Images were commonly available for the region every 30 minutes with hourly time stamps at minutes 08 and 38. When Rapid Scan Operations were required, i.e. severe weather conditions in the Caribbean area, only tri-hourly or hourly images were available. Further, as the 30 minutes scan and the 3 hours scan (time stamp at minute 45) coexisted, there are 8 times per day in which consecutive images can have 7 minutes time difference. This irregular availability was solved by the new GOES-R satellite, which started its operation in the year 2018, providing regular 15 minutes images for the continent (and recently 10 minutes images).

For this work only consecutive images separated by 30 minutes are considered from the 2016-2017 GOES13 period. The present time image and the previous image are used to derive the CMV. The solar forecast is performed for hourly time steps from the present time image time stamp. This imply that the hourly ground measurements integrals need to have the same time stamp of the satellite images and were calculated ad-hoc for the sake of this forecast assessment. The use of 30 minutes rate satellite images is an important difference with other implementations of CMV forecast in Europe (Lorenz et al., 2004) or USA (Perez and Hoff, 2013) where 15 minutes images are used.

3. Methodology

As previously explained, the general satellite forecast methodology consist in detecting the cloud movement (the CMV) from two consecutive satellite images and extrapolate it to the future, predicting the next images. Then, using a satellite-based solar estimation model the predicted image can be converted into a solar irradiation forecast. The similarity technique developed by Lorenz et al. (2004) is the main method currently used in the industry for satellite forecast. To estimate the cloud displacement in each pixel, the algorithm considers its surrounding rectangular area in the current image (called target area) and compares it with the neighbouring regions in the previous image inside a bigger search area (Kühnert et al., 2013). Two grid spacing need to be defined: a grid to move the target area within the search area (called target grid) and a grid in where to estimate the velocity field (called vector grid). The size of the search area and the resolution of both grids are limited due to computational cost. The similarity metric between regions is the root mean square deviation (RMSD). Once

the area which has the smallest RMSD in the comparison with the target area is identified, a motion vector is assigned to the pixel based on the translation. This methodology aim to identify areas with similar characteristics in both images, i.e. similar cloudiness patterns, so that the traslation of each target area is the CMV. The CMV derivation is the key element of this technique.

The size of the target area is selected following Kühnert et al. (2013), where the optimal target size is derived to be 110 × 110 km. By converting this kilometer specification to pixels for the regional satellite space resolution, a target area of 75 × 75 px is selected for this work. The size of the search area in relationship to the size of the target area defines the maximum cloud velocity that will be estimated. Slower cloud displacement are favoured as they lead to more stable and smooth velocity fields. Further, the larger the search area, the more mismatches can arise from the procedure, leading to artifacts and inaccuracies in the CMF. A maximum cloud velocity of 100 km/h is imposed here, which results in a maximum horizontal/vertical displacement of about 25 px in 30 minutes (the rate of the satellite images). For a square search area, this means a side length of l_s = 75 px + 25 px + (75/2) px ≈ 135 px, leading to a search area of 135 × 135 px. The grids for the CMV output (vector grid) and for the target displacement within the search area (search grid) need to be defined. For the vector grid, a similar resolution as Kühnert et al. (43 × 43 km) is used, leading to a pixel's spacing of 30 × 30 px. For the search grid a higher resolution spacing of 5 × 5 px is used. The vector and search grids are less dense than the image resolution due to the high computational time required to implement the methodology with denser grids. All these values are specified in Tab. 2. If a smooth continuous velocity field is assumed, which is usually desired, there is no much gain in performing a pixel by pixel similarity search and velocity estimation. Tests were made in order to check the sensibility of the forecast when modifying Tab. 2 parameters but the performance of the methodology was essentially the same. To avoid inaccuracies in the extrapolation of cloudiness structure with increasing time horizons, a CMV smoothing procedure is done as suggested by Kühnert et al. (2013). In our case, the CMV is averaged in a 3 × 3 pixels region in the vector grid. Using this output, the CMV is linearly interpolated into the denser image resolution grid so that it can be used to forecast the next images.

Tab. 2: Pixels size of search and cell regions and pixels grid step.

region	grid space	region size
search	5 × 5 px	135 × 135 px
target	30 × 30 px	75 × 75 px

Forecast was generate from 1 to 5 hours ahead for the available 30-minutes images in the 2016-2017 period. The predicted images are converted to a GHI forecast using an empirical estimation model presented in Alonso-Suárez et al. (2012). This model has a negligible mean bias and a relative RMSD of 12-13% for hourly solar resource assessment in the region. The reference persistence procedure applied here is the result of assuming that the clearness index k_T remains constant in time, defining it as $k_T = \frac{I_h}{I_{oh}}$ where I_h is the hourly GHI measurement and I_{oh} is the hourly solar irradiation at an horizontal plane in the top of the atmosphere. Thus, persistence forecast assumes that $k_T\ (t + \Delta t)\ =\ k_T(t)$ which results in:

$$\hat{I}_{h,\Delta t}^{per}(t) = k_T(t) \times I_{oh}(t + \Delta t) \qquad \text{(eq. 1)}$$

where $\hat{I}_{h,\Delta t}^{per}$ is the hourly solar irradiation persistence calculated at time (t) for a forecast time horizon Δt. In a similar way, we denote the CMV hourly solar irradiation forecast at time (t) for a time horizon Δt as $\hat{I}_{h,\Delta t}^{cmv}$. Errors in time (t) of the forecast are obtained from comparing the predicted value with the measured value as:

$$e_{t+\Delta t}(t) = \hat{I}_{h,\Delta t}(t) - I_h(t + \Delta t) \qquad \text{(eq. 2)}$$

so, positive deviations correspond to a GHI overestimation and negative deviations correspond to a GHI subestimation. The performance metrics used for evaluation are the Mean Bias Deviation (MBD), the RMSD and the Forecasting Skill (FS). These metrics are defined in the Eqs. (3), (4) and (5), respectively. The relative values of the MBD and RMSD are expressed as a percentage of the hourly measurements average and are denoted as rMBD and rRMSD, respectively. The FS quantifies the gain of the method as compared to the persistence procedure and will be also expressed as a percentage.

$$MBD_{\Delta t} = \frac{1}{N}\sum_{t=1}^{N}(\hat{I}_{h,\Delta t}(t) - I_h(t+\Delta t)) \quad \text{(eq. 3)}$$

$$RMSD_{\Delta t} = \sqrt{\frac{1}{N}\sum_{t=1}^{N}(\hat{I}_{h,\Delta t}(t) - I_h(t+\Delta t))^2} \quad \text{(eq. 4)}$$

$$FS_{\Delta t} = 1 - \frac{RMSD_{\Delta t}^{cmv}}{RMSD_{\Delta t}^{per}} \quad \text{(eq. 5)}$$

4. Results

The performance evaluation is shown in Tab. 3. Metrics are shown for site and regional forecast. Site forecast performance is calculated by averaging each metric over all sites. The regional forecast is assessed by comparing the average predicted GHI with the average measured GHI across the seven sites. Mean GHI value for site normalization is of 457 Wh/m^2 and for regional normalization is of 489 Wh/m^2 (this difference is because the number of hourly samples in each station is not the same). Similar MBD values are observed for site and regional forecast for each time horizon and each forecast strategy (CMV and persistence). Considering both spatial domains (site and regional), MBDs are low, both for the CMV forecast and the persistence procedure, being negative for the persistence (between -1.0% and -4.8%) and mostly positive for the CMV forecast (between -0.4% and +1.2%). The rRMSD trends for site and regional forecast are shown in Fig. 2 (a) and (b), respectively. In Fig. 2 (a) the shade correspond to one standard deviation of the inter-site rRMSD variability. As expected the rRMSD values are lower for regional forecast than for site forecast (plots have the same y axis scale). The performance of the CMV forecast is better than the persistence procedure in both spatial domains and for all hourly time horizons, exhibiting the typical increasing trends. For site CMV forecast the rRMSD obtained for the first time horizon (1 hour ahead) is of 18.7% (the lowest), which is around 6% above (in rRMSD) the hourly solar satellite site assessment uncertainty for the region. For regional CMV forecast the rRMSD obtained for 1 hour ahead is similar to that of the persistence procedure (but lower), being of 8.7% for the CMV and of 9.2% of the persistence. The rRMSD monotonically increases with the time horizon up to 37.0% for site CMV forecast and up to 17.7% for regional CMV forecast, at 5 hours ahead.

FS for site and regional CMV forecast are illustrated in Fig. 3. Positive FS are obtained for all hourly time horizons for both spatial domains. The regional FS is higher than the site FS for 2 hours ahead and above, but is lower for 1 hour ahead. Site forecast peaks at 2 hours ahead, reaching a maximum FS of +15.9%. Above the 2 hours ahead the site FS decreases till +10.6% at 5 hours ahead. On the other hand, the regional FS increases quickly from the first to the second time horizons, reaching an asymptote around +30% for 3 hours ahead and above. It peaks exactly at FS = +30.0% at 4 hours ahead, but the value is almost the same for 3 and 5 hours ahead.

Tab. 3: Performance metrics for site and regional forecast.

	Site forecast					**Regional forecast**				
	Persistence		**CMV forecast**			**Persistence**		**CMV forecast**		
time horizon	**MBD** (%)	**RMSD** (%)	**MBD** (%)	**RMSD** (%)	**FS** (%)	**MBD** (%)	**RMSD** (%)	**MBD** (%)	**RMSD** (%)	**FS** (%)
1 hour	-1.0	20.8	-0.4	18.7	+10.1	-1.0	9.2	+0.3	8.7	+5.4
2 hours	-2.7	30.2	+0.2	25.4	+15.9	-2.4	15.0	+0.6	11.1	+26.0
3 hours	4.4	36.5	+0.5	31.1	+14.8	-3.9	19.8	+0.7	13.9	+29.8
4 hours	-5.2	40.1	+0.9	34.8	+13.2	-4.7	23.3	+0.9	16.3	+30.0
5 hours	-4.8	41.4	+1.2	37.0	+10.6	-4.6	25.2	+0.9	17.7	+29.8

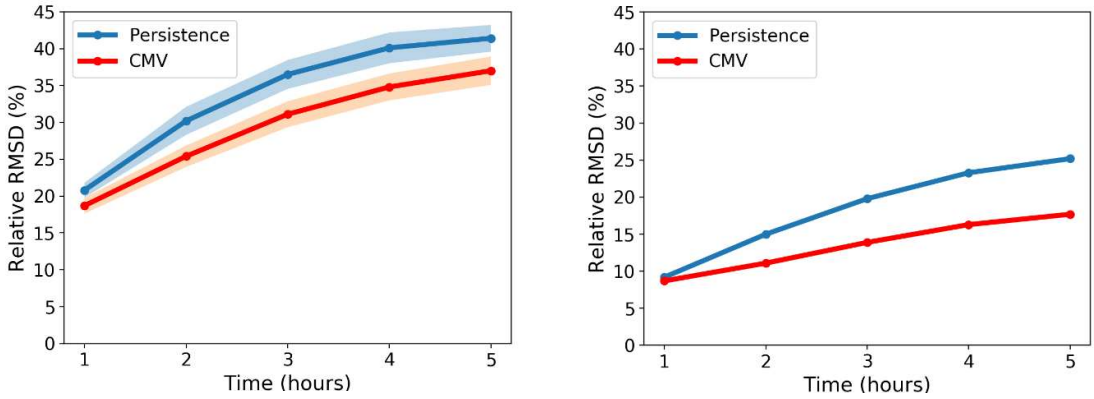

(a) Site forecast. **(b) Regional forecast.**

Fig. 2: Relative RMSD performance metric vs time horizons.

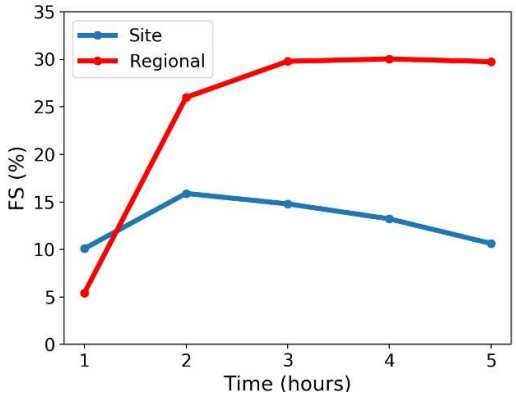

Fig. 3: Forecasting skill metric for site and regional forecast.

In Fig. 4 the scatter plots between the CMV forecast and the measurements are provided for 1, 3 and 5 hours ahead time horizons. Two aspects can be seen: (i) the scatter plots and their linear regression show a low deviation from the $x = y$ perfect agreement line (the slopes are ≈ 1), confirming the low MBD found above, and (ii) the dispersion in the plots increase with the time horizon, confirming the increasing RMSD trend. In general, the scatter plots show a good agreement between the predicted and measured GHI values, downgrading as the time horizon increase.

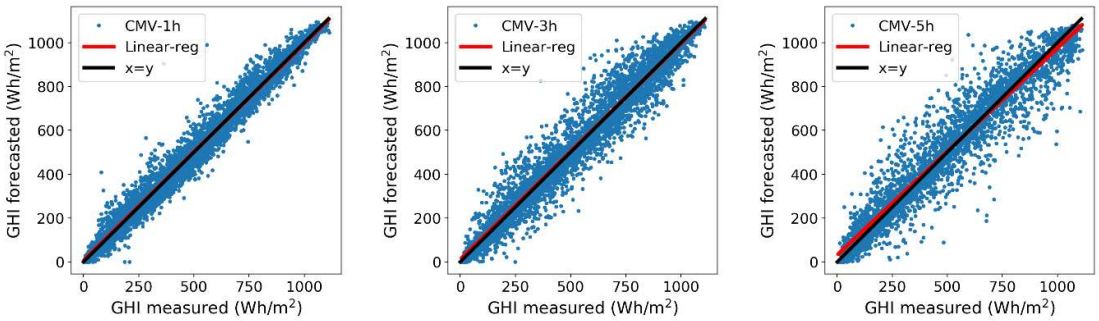

(a) Forecast horizon: 1 hour ahead. **(b) Forecast horizon: 3 hours ahead.** **(c) Forecast horizon: 5 hours ahead.**

Fig. 4: Scatter plots between the CMV predictions and the measurements for different time horizons.

For further understanding the CMV performance, Fig. 5 shows the rMBD (a) and rRMSD (b) for 1 hour ahead forecast discriminated by the moment of the day (using the cosine of the solar zenith angle, $\cos\theta_z$) and by the cloudiness (using the clearness index, k_T). These diagrams are done using together the time-series of the predicted and measured irradiation in the seven stations, so they represent the site forecast performance. The higher deviations are observed for two situations: (i) intermediate cloud cover conditions ($0.3 \leq k_T \leq 0.6$) during summer and middle season middays ($\cos\theta_z \geq 0.8$) and (ii) low turbidity clear sky conditions (first upper row of the diagrams). For instance, it can be seen that the higher positive rMDB are found in the first situation (≈ +10%) and the higher negative rMBD are found in the second situation (≈ -10%). For the rest of the diagram the rMBD remains low, in most cases between ±5%. Also, the rRMSD is higher (and similar) under these two situations, being around 25-30%. The general trend of rRMSD is to decrease with decreasing cosine of solar zenith angle. The rRMSD diagram exhibits similar pattern to the one presented by Lorenz et al. (2009) for the evaluation of the ECMWF Numerical Weather Predict forecast over more than 200 meteorological stations in Germany. The diagrams are also similar to those observed for satellite-based irradiation assessment in the region (Alonso-Suárez, 2017). In fact, the deviations observed at low turbidity clear sky conditions are a drawback of the assessment model being used rather than the CMV forecasting methodology. To isolate the deviations introduced by the CMV methodology from the deviations introduced by the solar satellite assessment model will be part of future work.

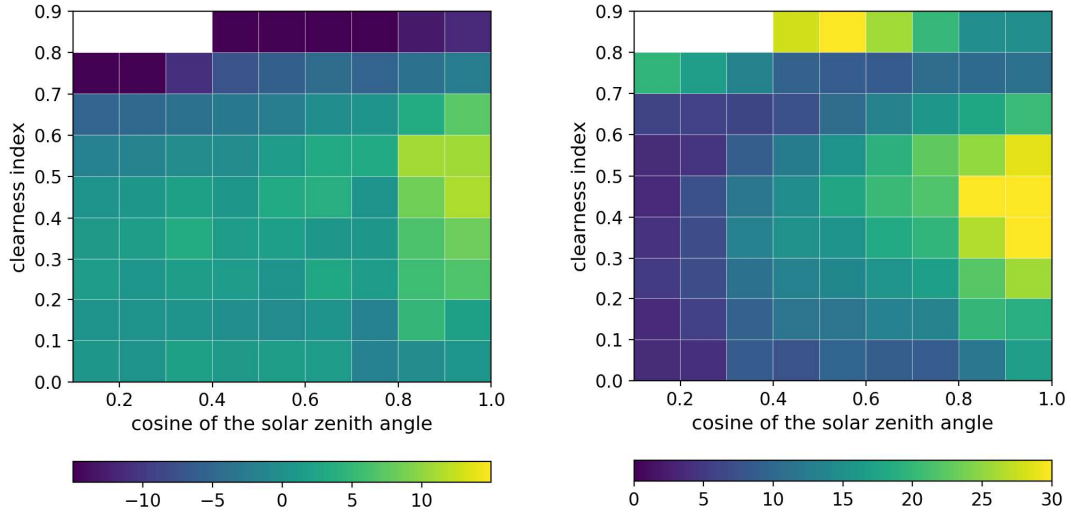

(a) Site rMBD diagram. **(b) Site rRMSD diagram.**

Fig. 5: Site performance for 1 hour ahead CMV forecast discriminated by cosine of the solar zenith angle and clearness index.

5. Conclusion

The CMV satellite forecasting technique proposed by Lorenz et al. (2004) was implemented and evaluated for 1 to 5 hours ahead GHI forecast in the Uruguayan territory, a representative part of the broader Pampa Humeda region of the south-east of South America. The method outperforms the classical persistence for all time horizons, both for site and regional forecast, showing lower rRMSD and low bias, resulting in positive FS values. The FS of the site forecast increases from 1 to 2 hours ahead, peaking at the latter at ≈ +16%, but then decreases with increasing forecast horizon. The FS of the regional forecast increase quickly in the first two time horizons and it remains approximately constant around +30% from 3 to 5 hours ahead. The FS for regional domain is significantly higher than over specific sites from 2 to 5 hours ahead. For 1 hour ahead this does not hold, and the FS of site forecast is better that the regional forecast. Results are similar to those found in Kühnert et al. (2013) and Perez and Hoff (2013) for the German and USA territories, respectively, although 30-minutes images are used here (which are the images available for South America for 2016-2017 period) instead of 15-

minutes images. Results from this techniques are promising for the region and the next step is to assess the performance for PV power forecast, which require a model to transpose the GHI to tilted plane and a PV power plant model to estimate the plant's power output.

6. References

ADME, (2018). Informe Anual 2018. Technical Report, Administración del Mercado Eléctrico, Uruguay.

Alonso-Suárez, R., Abal, G., Siri, R., Musé, P., (2012). Brightness-dependent Tarpley model for global solar radiation estimation using GOES satellite images: Application to Uruguay, Solar Energy 86(11):3205-3215.

Alonso-Suárez, R. (2017). Estimación del recurso solar en Uruguay mediante imágenes satelitales. Ph.D. thesis Facultad de Ingeniería, Universidad de la República.

Gurín, M., Cornalino, E., Guggeri, A., Alonso-Suárez, R., Giacosa, G., Abal, G., Terra, R., Chaer, R., (2016). Complementariedad de los recursos renovables (solar--eólico) y su correlación con la demanda de energía eléctrica. Technical Report MIEM-DNE 005-2016, Facultad de Ingeniería, Udelar, Uruguay.

Kühnert, J., Lorenz, E., y Heinemann, D., (2013). Chapter 11 - Satellite-based irradiance and power forecasting for the German energy market. In Kleissl, J., editor Solar Energy Forecasting and Resource Assessment, pp. 267-297, Academic Press, Boston.

Lorenz, E., Hammer, A., y Heinemann, D., (2004). Short term forecasting of solar radiation based on satellite data, Proceedings of the EUROSUN2004 (ISES European Solar Congress), pp. 841-848, Freiburg, Germany.

Lorenz, E., Hurka, J., Heinemann D., Beyer, H. G., (2009). Irradiance Forecasting for the Power Prediction of Grid-Connected Photovoltaic Systems, IEEE Journal of Selected Topics in Applied Earth Observations and Remote Sensing 2(1):2-10.

Pedro, H., Coimbra, C., (2012). Assessment of forecasting techniques for solar power production with no exogenous inputs, Solar Energy 86(7):2017-2028.

Peel, M. C., Finlayson, B. L., Mcmahon, T. A. (2007). Updated world map of the köppen-geiger climate classification. Hydrology and Earth System Sciences Discussions 11:1633-1644.

Perez, R. y Hoff, T. E., (2013). Chapter 10 - SolarAnywhere forecasting. In Kleissl, J., editor, Solar Energy Forecasting and Resource Assessment, pp. 233-265. Academic Press, Boston.